AIAA JOURNAL
Vol. 47, No. 7, July 2009

Phase Synchronization of Vortex Shedding from Two Circular Cylinders Using Plasma Actuators

Asad Asghar*
Royal Military College of Canada, Kingston, Ontario K7K 7B4, Canada
and
Eric J. Jumper†
University of Notre Dame, Notre Dame, Indiana 46556

DOI: 10.2514/1.34580

Plasma actuators were used to phase synchronize vortex shedding from two side-by-side circular cylinders in the Reynolds number range of $Re_d = 16,700–76,500$. The two cylinders were installed perpendicular to the flow, with the pitch to diameter ratio of 4. The natural vortex shedding for this spacing is known to be, predominantly, out of phase. Plasma actuators were installed on the sides (±90 deg from the forward stagnation point) of each cylinder along the full span in two configurations. These actuators, by the formation of plasma, produced an air jet in the downstream direction. The vortex-shedding phase between the two cylinders was determined from unsteady velocities measured by two hot wires, located behind the cylinders at identical relative positions with respect to the center of each cylinder. The cross correlation of the two hot-wire signals showed the effectiveness of the plasma actuators in synchronizing the vortex shedding. The correlation coefficients of +0.4 to +0.6 (or −0.6 to −0.4) were obtained when the plasma actuators were activated, showing the in-phase (or out-of-phase) synchronization of the vortex shedding. The capability of the plasma actuators for the arbitrary phase synchronization of the vortex shedding was also demonstrated. The ability of the plasma actuators to phase synchronize vortex shedding depends on input power as well as actuator design.

Nomenclature

c	=	airfoil or vane chord
d	=	diameter of cylinder
f	=	frequency, Hz
f_s	=	vortex-shedding frequency, Hz
L	=	length of cylinder
P	=	distance or pitch between cylinder centers
Re_d	=	Reynolds number based on diameter
S	=	spacing between cylinders
x	=	streamwise distance or coordinate
y	=	perpendicular to streamwise coordinate
π	=	angle in radians equivalent to 180 deg

I. Introduction

FLOW around circular cylinders has been studied extensively due to its widespread engineering applications and associated problems of flow-induced vibration, wake turbulence, noise, and drag forces on bodies. Examples of flow around circular cylinders can be found in bridges, offshore structures, transmission lines, heat exchangers, nuclear reactors, and aircraft appendages. The review article of Williamson [1] and the book by Zdravkovich [2] provide a comprehensive review of the theoretical and experimental research done on the flow around circular cylinders during the last century.

Many researchers [3] have investigated different approaches to controlling vortex shedding behind circular cylinders; their objectives have been directed at suppressing the vortex shedding, separation control, and lock-in or synchronization of the shedding. The ability to control the vortex shedding can be used to reduce drag, increase lift, suppress noise, decrease vibration, and increase mixing or heat transfer. The method of control depends on the objective as well as the Reynolds number of the flow. To control the vortex shedding, researchers have considered both active and passive control schemes in their investigations. Many investigators have also used feedback in their control loops [3].

Flow around multiple cylinders is of practical significance. It occurs in heat exchanger tubes, arrays of nuclear fuel rods, and offshore structures, etc. The flowfield around two or more side-by-side cylinders in a crossflow is somewhat different from the flow around a single cylinder because of the influence of one on another. Figure 1 shows the definition of the various terms used in the multiple cylinder flow. The flow patterns observed around two side-by-side cylinders can be generalized into four distinct flow regimes with the separation, P/d or S/d, between them being the characterizing parameter. When the separation between the cylinders is large, that is, $P/d > 5–6$, the flow behind each cylinder is relatively oblivious to the presence of the other cylinder and behaves like a single cylinder flow. When the spacing is reduced, the interaction between the cylinders gradually occurs. The interaction is relatively weak for the

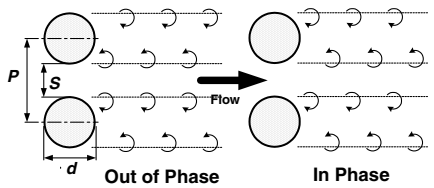

Fig. 1 Phase of vortex shedding from two side-by side cylinders in crossflow.

Presented as Paper 0925 at the 42nd Aerospace Sciences Meeting and Exhibit, Reno, Nevada, 4–7 January 2004; received 17 September 2007; revision received 25 July 2008; accepted for publication 19 September 2008.

*Assistant Professor, Department of Mechanical Engineering; formerly Graduate Research Assistant, Hessert Laboratory for Aerospace Research, University of Notre Dame, Notre Dame, IN 46556. Member AIAA.

†Professor, Center for Flow Physics and Control, The Hessert Laboratory for Aerospace Research, Department of Mechanical Engineering. Fellow AIAA.

spacing $2 < P/d < 6$. In this weak range, the vortex shedding remains similar to that found behind an isolated cylinder; however, some phase synchronization does occur between the cylinders. The vortex streets may synchronize out of phase (i.e., when vortices of opposite signs are shed simultaneously on opposite sides of the cylinders, as described in Fig. 1). Alternatively, in-phase vortex-shedding synchronization may occur. In fact, the vortex shedding can and does switch between the out-of-phase and in-phase shedding; however, the shedding is predominantly out of phase. When the spacing between the cylinders is further reduced to $1.1 < P/d < 2$, a grossly unsteady flip-flopping occurs between two quas-istable, asymmetric states. When the spacing between the cylinders is reduced to $P/d \approx 1$, a single wake is observed behind the cylinders [4]. The natural flow pattern behind two cylinders can also be modified using various flow-control mechanisms [5].

The present set of experiments was conducted in an effort to synchronize the vortex-shedding phase from two side-by-side circular cylinders in a low-speed subsonic flow. The necessity of carrying out these experiments originated from earlier experiments in compressible-flow cascade, in which vortex shedding from multiple circular cylinders was used to produce upstream-propagating, unsteady potential disturbances [6–9]. In the compressible-cascade experiments that were performed to investigate the interaction of these potential disturbances with the trailing edge of an unloaded cascade vane, the response of the vane to the downstream forcing did not appear to be caused by a well-conditioned potential disturbance. The subsequent investigation into the cause of this behavior pointed to the fact that the forcing disturbances, produced by the vortex shedding from the downstream row of cylinders, were not in phase, and were in fact, not only "out of phase" but continuously changing their phase relationships.

After trying many passive methods of creating in-phase vortex shedding from circular rods, we decided that some sort of active control of vortex shedding was necessary. This control should be such that it can force vortices to shed in phase. While we were searching for the active-control methods for controlling the vortex shedding, the plasma research group at Notre Dame [10,11] successfully demonstrated the potential of surface dielectric barrier discharge or plasma actuators to control flow. These actuators have no moving parts and perform well at high (3–10 kHz) frequencies (see next section). Therefore, we decided to use the plasma actuators for controlling the vortex shedding from the multiple cylinders.

Because our goal was to control the phase of shedding from multiple rods, the minimum number of rods required for testing was two. Further, developing a forcing strategy at high speed for small cylinders appeared too challenging for initial studies of this kind. As discussed further in detail in [12], these first studies retained relevance to the original objective by setting, as a goal in the lower-speed studies, a match to the cascade's Reynolds number. To these ends, two side-by-side cylinders were placed in a low-speed flow and the Reynolds number in the low-speed tests was kept in the range of the compressible-flow cascade tests by using bigger diameter cylinders in the low-speed tests.

II. Flow Control Using Plasma Actuators

In the present research, plasma actuators were used for the phase synchronization of vortex shedding from two side-by-side circular cylinders. A plasma actuator is a form of dielectric barrier discharge (DBD) that can sustain large-volume discharge at atmospheric pressure, without the discharge's collapse into a constricted arc [13–16]. Dielectric barrier discharges in various forms are already being used for other (nonflow control) applications such as ozone production and surface treatment [17]. The interest in using dielectric barrier discharge for flow-control application has increased in the last few years [18–22]. Recent review articles by Moreau [23] and by Corke et al. [24] provide a comprehensive review of the research done on the characterization and flow-control application of the DBD in the last decade. Because the plasma in the flow-control application is formed over a dielectric surface, plasma actuators are also called surface dielectric barrier discharges. In this paper, these actuators will be called "single dielectric barrier discharge" (SDBD) actuators or for brevity, plasma actuators.

The actuators used for this research consisted of one encapsulated electrode completely covered with dielectric material (for example, Kapton® polyamide film) and an upper electrode exposed to the surrounding air. Typically, the electrodes are thin (≈1–2 mil or 25.4–50.8 μm) and long in the spanwise direction. When an ac voltage in the amplitude range of 5–10 kV with high frequency (3–10 kHz) is applied to these electrodes, a plasma discharge appears over the dielectric surface above the insulated electrode as shown in Fig. 2 and directed momentum is coupled into the surrounding air [13,14,18,23,24]. The air jet produced by this momentum coupling has been shown to have velocities up to 3–4 m/s in still air [18,23] and to be useful for applications such as drag reduction and reattachment of separated flows [19–24].

The mechanism through which the plasma actuators affect the flow can be found in some detail in the review article by Corke et al. [24]. The plasma, consisting of charged particles (ions), is formed above the encapsulated electrode as the result of a series of discharges as electrons are transferred from exposed electrodes to the dielectric surface above the encapsulated electrode during the negative-going phase of the applied ac cycle and vice versa during the positive-going phase of the ac cycle. The charged particles in the plasma impart momentum into the flow through interaction with the electric field. Basically, plasma actuators create a body force on the volume of fluid within the region of the plasma that first draws the flow down to the exposed surface of the actuator and then relieves the accumulation of fluid as a jet directed along the encapsulated electrode very close to the surface imparting a fixed amount of momentum into the jetted fluid associated with the amplitude and frequency of applied ac voltage. Although the body force always imparts momentum in the direction of the asymmetry of the actuator (see Fig. 2), the efficiency of the body-force coupling into the fluid is greater for the current (i.e., electrons) leaving the exposed electrode and imbedding into the dielectric than for the return cycle that pulls the electrons out of the dielectric providing a current back to the exposed electrode [24]. The performance of the actuator depends strongly on the charges in the plasma and the interelectrode electric field [18]. Therefore, applied ac voltage and actuator design are the critical factors in the operation of the SDB plasma actuators. Further information about the effect of applied voltage on the induced flow can be obtained in [18,23–26]. The electrohydrodynamic force produced by the plasma actuator and the resulting fluid motion has been theoretically and computationally investigated by Enloe et al. [18], Shyy et al. [27], Orlov [28], Font [29], Boeuf and Pitchford [30], and Roy and Gaitonde [31].

III. Experimental Setup and Procedure

The experiments in the present study on phase synchronization of vortex shedding were conducted in one of two 2×2 ft^2 low-speed, in-draft wind tunnels in the Hessert Laboratory at the University of Notre Dame. The freestream turbulence intensity in the test section was less than 0.1%. Two circular cylinders of diameter $d = 1.5$ in. and length-to-diameter ratio L/d of 8 were used. The cylinders were installed horizontally, perpendicular to the flow, side by side in the test section with pitch-to-diameter ratio P/d of 4. This spacing was chosen because it was midway in the practical range contemplated for use in the compressible-flow cascade and, as previously

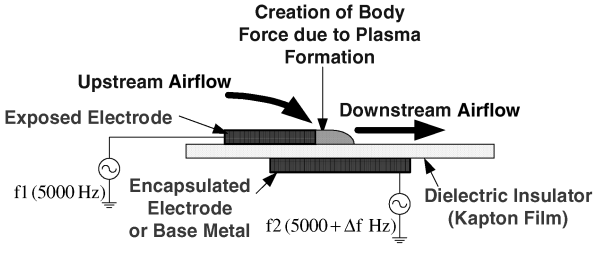

Fig. 2 Schematic of effect of SDBD, or plasma actuator, on airstream.

described, placed the natural shedding of the cylinders in the weak-interaction regime, where the shedding is predominantly π out of phase. Figure 3 shows two schematic views of the test setup. Two end plates were used to reduce the end effects on the cylinders and to keep nominally two-dimensional flow on the midspan of the cylinders. The end plates were designed according to the guidelines provided by Szepessy [32] and Stansby [33]. The end plates were attached rigidly to the roof and floor of the test section. The wind-tunnel blockage with two cylinders was 8.3%; as such, blockage correction was deemed unnecessary.

During this research, many actuator configurations were tried to achieve vortex-shedding control up to the target $Re_d = 76,500$. The configurations are denoted by letters A–F. The earlier configurations (A–D) of plasma actuators had limited effectiveness or were effective at low Reynolds number only. The test setup and the results for the plasma actuator configurations A–D are presented in [34,35]. In this paper, we will discuss the results for the plasma actuator configurations E and F only, as shown in Fig. 4. The arrows in Fig. 4b show the direction of jetting of the plasma actuators. Configurations E and F were effective up to (relatively) higher Reynolds number or up to the target Reynolds number. The plasma actuator configurations on the two cylinders of each configuration were kept identical to avoid any asymmetric effects. The cylinders were made of Teflon for the plasma actuator configuration E and of aluminum for configuration F. When the aluminum cylinder was used, it also acted as the encapsulated electrode. Four layers of 2-mil Kapton film were wrapped on each aluminum cylinder before installing the exposed electrodes. Note that 2-mil Kapton film tape has an approximately 1.7-mil silicon-adhesive layer on its back, producing a total tape thickness of approximately 3.7 mil (e-mail communication with 3M and Parmacel). For configuration E, the encapsulated electrode on each (Teflon) cylinder was made by installing copper foil strips of 1.5-mil thickness on the leeward side of the cylinder, from $+80$ deg from the forward stagnation point (FSP) to -80 deg from the FSP; the encapsulated electrode was isolated from the exposed electrodes by four layers of 2-mil Kapton film. In both the configurations, copper foil strips of 1.5-mil thickness and 1/8-in. width were used for exposed electrodes and were installed along the full span of the cylinder, except for three-fourth inch from the ends to avoid arcing between the encapsulated and exposed electrodes (see Fig. 4a). For configuration E, the exposed electrodes were installed in such a way that the plasma formed at ± 90 deg from the FSP (see Fig. 4b). As described by Asghar and Jumper [34], better phase synchronization of the vortex shedding was obtained when the plasma actuators were close to the sides, ± 90 deg to ± 110 deg from the FSP. For configuration F, two plasma actuators on each side of the cylinder were used (see Fig. 4b) to provide more jetting to the flow, close to the separated shear layers. Enloe et al. [18] demonstrated that the effect of multiple actuators is additive if they are placed in reasonably close proximity. The exposed electrodes in configuration F were installed in such a way that the plasma formed at ± 80 deg and ± 110 deg from the FSP. The formation of the plasma at the upstream edge of the exposed electrode was suppressed by covering the edge with multiple layers of 2-mil Kapton film. The

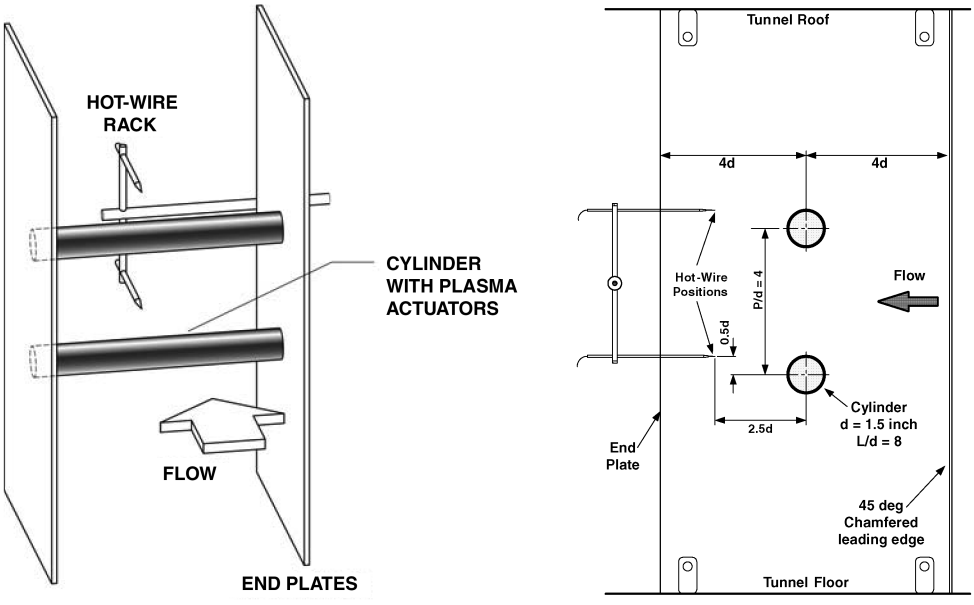

a) 3-D schematic (looking downstream) b) Side-view schematic

Fig. 3 Test setup for phase synchronization of vortex shedding from two side-by-side cylinders.

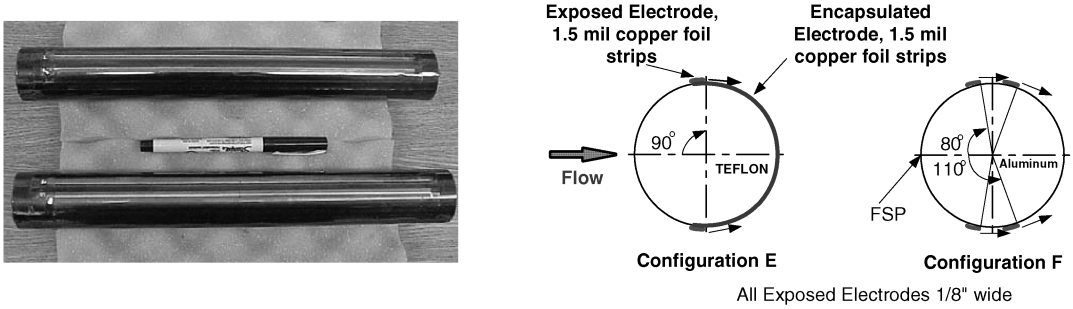

a) Spanwise view b) Schematic of cross section

Fig. 4 Configurations E and F of plasma actuators on cylinder.

whole configuration was made in such a way that the step changes in the diameter of the cylinder and large surface roughness on the cylinder were not present.

In the tests, each exposed electrode was connected to a high voltage of $f1 = 5000$ Hz frequency, and the encapsulated electrodes were powered with a high voltage of $f2 = 5000 + \Delta f$ Hz frequency (see Fig. 2). The differential frequency Δf was kept the same as the "natural" vortex-shedding frequency f_s, corresponding to the flow velocity or the center frequency of the two cylinders. This method of forcing generated plasma by voltage-amplitude modulation at the natural vortex-shedding frequency. Six high-frequency, high-amplitude voltage generators were made for exciting the plasma actuators as shown in the schematic of Fig. 5. A low-amplitude, waveform signal from a function generator (Agilent 33120 A) was first supplied to a variable-gain amplifier (Crown CE 2000). The amplified voltage was then fed into the primary coil of a 1:137 transformer (Corona Magnetics, CMI-5012) to increase the voltage-amplitude level to the 5–10 kV range. The high voltage for the excitation of the plasma actuators was obtained from the secondary coil of the transformer. Three high-voltage generators were used for the in-phase and out-of-phase forcing, as shown in Fig. 6, and six were used for the arbitrary phase forcing. The function generators of the high-voltage generators could be mutually synchronized to produce the ac voltage with arbitrary phase between them.

The unsteady velocity behind each cylinder was measured using straight hot-wire (Dantec 55P01) probes placed at distances of $x/d = 2.5$ and $y/d = 0.5$, downstream of each cylinder center, as shown in Fig. 3b. These positions of the hot-wire probes were selected because of two reasons. First, we wanted to place the hot-wire probes at the positions where the presence of the fully formed vortex and the large fluctuation in the velocity were expected [35]. Second and more important, we placed hot-wire probes where the interference from the plasma actuators would not be an issue. At this position of the hot-wire probes, we did observe large amplitudes in the unsteady velocity, assuring good signal-to-noise ratio [35]. The hot-wire probes were operated in the constant-temperature mode using a TSI IFA-100 anemometer. The tests were made in the Reynolds number (based on cylinder diameter) range from 16,700 to 76,500, corresponding to the freestream velocity of 6.5–30.5 m/s. For all the runs, approximately 4.1 s of velocity data were collected at a sampling rate of 2–4 kHz (8192–16,384 samples) depending upon the flow velocity. Because the experiment involved the correlation of velocity associated with the shedding and not higher frequency velocity fluctuations, the velocity signals were low pass filtered at 100–300 Hz depending upon the shedding frequency. The velocity data were collected first without operating the plasma actuators and then with exciting the flow by the plasma actuators. This approach provided an effective method for comparing the natural and controlled vortex-shedding environment. The hot-wire signals for the uncontrolled case were also used to determine the natural Strouhal shedding frequency f_s at each tunnel run. The average vortex-shedding frequency was determined by the Fourier transformation of the velocity signal of each cylinder. The natural shedding frequency was then used to drive the plasma actuators that were operated with the differential frequency (Δf) between the encapsulated and exposed electrodes, as described previously.

A. Flow-Visualization Setup

The global picture of the flow behind the two cylinders with and without control was obtained by injecting smoke (kerosene or polypropylene glycol vapors) into the test section. The flow pattern was made visible by a thin sheet of laser light. Flow visualization on the cylinders of configuration E was done with a continuous argon–ion laser (Coherent Innova 70) and on the configuration-F cylinders with a pulsed argon–ion laser. An optical chopper (DigiRad C-980)

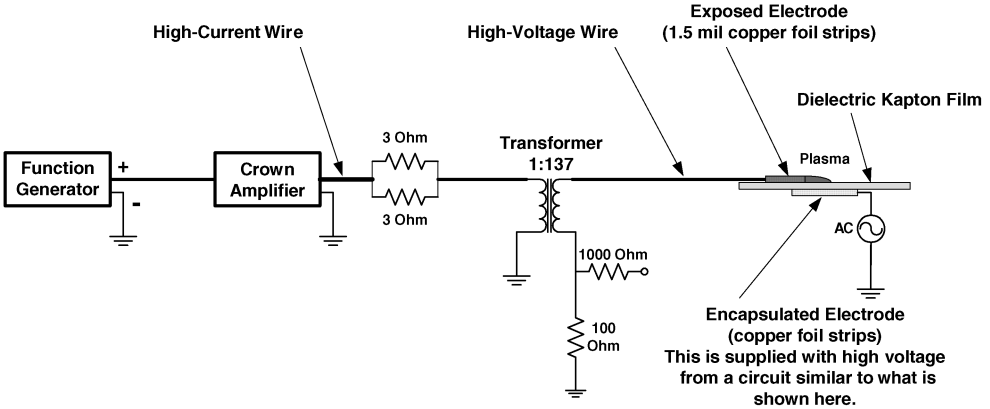

Fig. 5 Schematic of electronic circuit of high frequency and high-voltage generator.

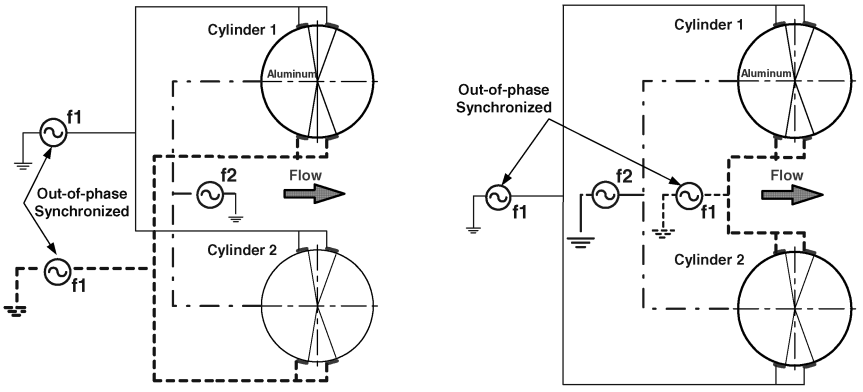

a) In-phase forcing **b) Out-of-phase forcing**

Fig. 6 Forcing of two cylinders to produce in-phase and out-of-phase vortex shedding.

Table 1 Estimated total uncertainty in various measurements and calculated variables

Measurement/variable	Nominal value and uncertainty
Cylinder diameter	1.5 ± 0.01 in.
Reynolds number	$41,000 \pm 600$
Hot-wire location	95 ± 1 mm
Vortex-shedding frequency	84 ± 2 Hz
Correlation coefficient	0.5 ± 0.04
Phase at zero time delay	0.012 ± 0.001 s

was used to pulse the laser at the vortex-shedding frequency. The flow visualization for configuration E was recorded using a video camera with a shutter speed of $1/60$ s (i.e, approximately at half the time period of vortex shedding at flow-visualization Reynolds number). The flow pictures were extracted from the video images using computer software after digitization of video images. Flow visualization for configuration F was recorded with a digital still camera using shutter speed long enough to capture several cycles of vortex shedding (i.e., several one-laser-pulse per-cycle captured, at the same phase angle, per shutter opening) without compromising sharpness of the image.

B. Estimated Uncertainty

The total uncertainty estimated in various measurements and calculated variables relevant to the results reported in this paper are given in Table 1.

IV. Results and Discussions

The unsteady velocities behind the two cylinders were used to determine the effect of the plasma actuators on vortex shedding. Figure 7 shows two typical time series of the unsteady velocities at $Re_d = 41,000$ with and without the plasma activation for configuration-F cylinders. The effect of exciting the flow with the plasma actuators is clearly seen by the phase difference between the two unsteady velocities as shown in Fig. 7. In Fig. 7a, for the plasma off, the velocities are essentially out of phase over the entire time series, and in Fig. 7b, for plasma on, the velocities are in phase. Note that in Fig. 7b, although the velocities are in phase, the amplitude fluctuations are still present and are similar to those in Fig. 7a. These amplitude fluctuations are the results of the irregularities that develop in the shear layer after the separation point and in the vortex during the formation process.

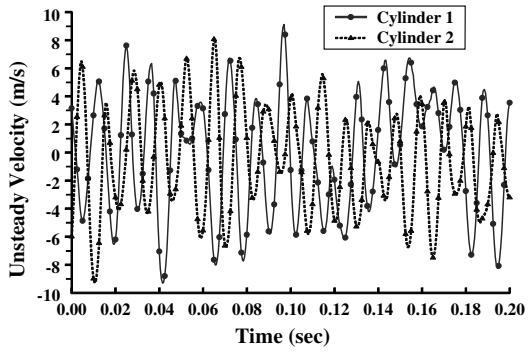

a) Plasma actuators off

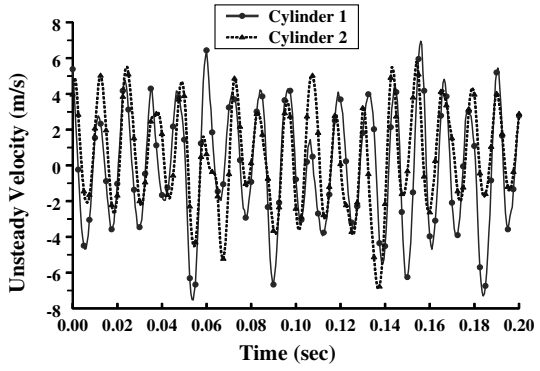

b) Plasma actuators on

Fig. 7 Unsteady velocity behind two cylinders: $Re = 41,000$.

The cross correlation of the unsteady velocity behind each cylinder was used to determine the phase between the vortex shedding from the two cylinders. The correlation coefficient at zero time delay is negative when the phase of the shedding is 180 deg out of phase and positive when the shedding is in phase. The actual value of the correlation would depend on the randomness of the phase between the shedding from the two cylinders. The approximate upper limit of the correlation of the unsteady velocities behind the cylinders was determined by taking the autocorrelation of the velocity behind one cylinder. The autocorrelation rapidly declined to $+0.55$ only after one cycle of vortex shedding, indicating natural wandering or the randomness of the frequency of vortex shedding [34,35]. Based on the autocorrelation, we consider a cross correlation of approximately $+0.40$ and above to represent in-phase vortex shedding. Figure 8 shows the cross correlation of the unsteady velocities shown in Fig. 7. The cross correlation in Fig. 8a of -0.15 at zero time delay for the uncontrolled flow indicates that the natural vortex shedding, with the spacing of $P/d = 4$, was mainly π out of phase. The maximum correlation in Fig. 8b of approximately $+0.6$ at zero time delay for the controlled case shows that the two velocities are in phase and, hence, show the effectiveness of the plasma actuators in synchronizing the vortex shedding. Moreover, the rapid decline in the correlation for the plasma-off case (see Fig. 8a) shows that the natural vortex shedding remains correlated for a very short duration, typically, for about 10 to 20 Strouhal periods; whereas, the decrease in the correlation for the plasma-on case, shown in Fig. 8b, is essentially nonexistent, demonstrating that the plasma actuators also decrease the fluctuations of the phase (or frequency wandering) of the vortex shedding. This reduction in the frequency fluctuation was also observed in the spectrum of the unsteady velocities behind the cylinders, as shown in Fig. 9. The spectrum was wideband

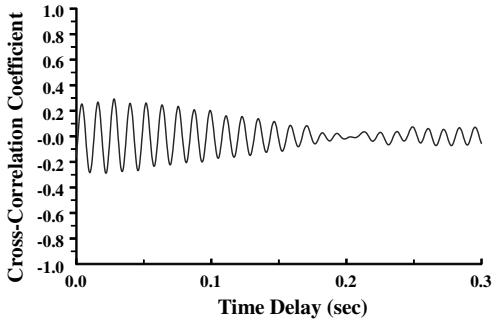

a) Plasma actuators off

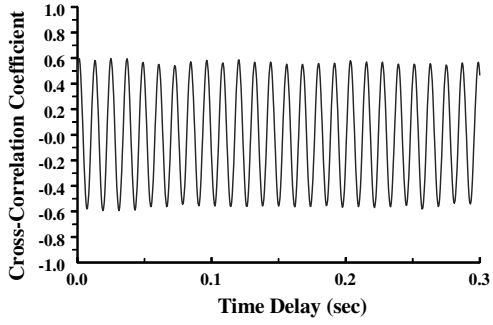

b) Plasma actuators on

Fig. 8 Cross correlation of unsteady velocities behind two cylinders: $Re_d = 41,000$.

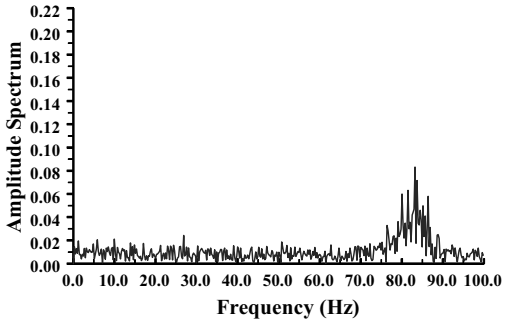

a) Plasma actuators off

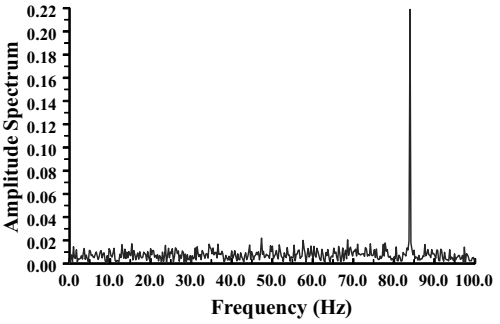

b) Plasma actuators on

Fig. 9 Spectrum of unsteady velocity behind a cylinder: configuration F, $Re_d = 41,000$.

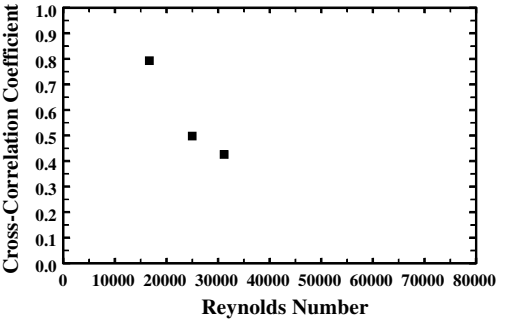

a) In-phase forcing, configuration E

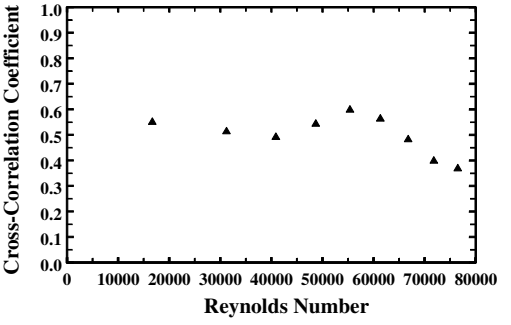

b) In-phase forcing, configuration F

Fig. 10 Cross-correlation coefficient at various Reynolds numbers with plasma actuators on.

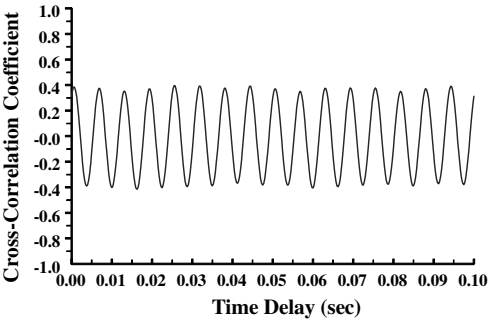

Fig. 11 Cross correlation of unsteady velocities behind two cylinders: plasma actuators on, $Re_d = 76,500$.

(centered on the Strouhal frequency) when the plasma was off (Fig. 9a) and narrowband when it was turned on (Fig. 9b), indicating lock-on. Similar levels of the phase synchronization and the reduction in the frequency wandering were observed at lower and higher Reynolds number [35].

As already discussed in the Introduction, our motivation for this work was to eventually use the plasma actuators in a weakly compressible cascade (Mach number ≈ 0.4–0.5). For this purpose the Reynolds number ($Re_d = 76,500$) for the forcing rods in the compressible cascade was the target Reynolds number for the cylinders in the low-subsonic flow. Various configurations of plasma actuators were tried in order to achieve phase synchronization up to this Reynolds number. The "effectiveness" of configurations E and F with variation in the Reynolds number is shown in Fig. 10. The plots show the cross-correlation coefficients for zero time delay. For the purpose of this discussion, effectiveness is measured by the magnitude of the zero-time-delay cross-correlation coefficient. The coefficients shown in Fig. 10 are the average values obtained for each forcing condition at the particular Reynolds number. It should be noted that the correlation coefficients depend strongly on actuator design, forcing frequency, power input, and flow velocities. While the configuration is held constant over the Reynolds number range for each plot, the other influences, such as applied voltage, change with Reynolds number, and, thus the plots cannot be interpreted as Reynolds-number-by-Reynolds-number direct comparison of effectiveness either between the configurations, or for any particular configuration. However, they do show the trend in at least the ability to synchronize the shedding for a particular configuration. For configuration E, for example, the correlation coefficient was $+0.79$ at $Re_d = 16,700$, but for configuration F, it was only $+0.55$ at the same Reynolds number (see Fig. 10b). Further, it is clear from Fig. 10a that configuration E was ineffective for Reynolds numbers above $Re_d = 31,200$. Referring to Fig. 4b, in an attempt to add "actuator authority," two actuators on each side were placed on the cylinders (i.e., configuration F) and tested. The correlations achieved with configuration F were in the range of about 0.40 to 0.6 for Reynolds number up to $Re_d = 76,500$. The correlation is close to $+0.40$ at $Re_d = 76,500$, as shown in Fig. 11. Although the phase synchronization at $Re_d = 76,500$ was less than perfect, the cross-correlation coefficient of $+0.40$ still shows the effectiveness of the plasma actuators at this Reynolds number. The decline in the correlation at a higher Reynolds number and, hence, the phase synchronization was due to the large difference in the vortex-shedding frequencies between the two cylinders [35].

As discussed in the Introduction, the natural, unforced vortex shedding from two side-by-side cylinders with a spacing of $P/d = 4.0$ is predominantly π out of phase. To investigate the effectiveness of the plasma actuators in promoting the π out-of-phase vortex shedding, we excited the electrodes in such a way that the vortices were forced to shed out of phase; that is, the applied voltage to the opposite side of the cylinders was in phase (see Fig. 6b). Figure 12 shows the correlation coefficient of the unsteady velocities behind the cylinders of configuration F for the π out-of-phase forcing. The forcing increased the negative correlation of the unsteady velocities and the out-of-phase synchronization of vortex shedding. The correlations are between -0.6 to -0.35 up to $Re_d = 72,000$. Thus, the character of the out-of-phase forcing experiments was essentially a mirror image of the in-phase forcing. As such, the discussion in the previous paragraph applies equally well to the out-of-phase experiments.

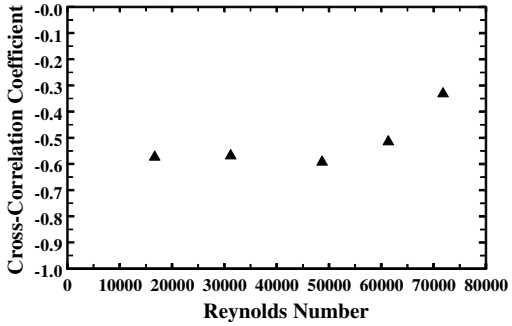

Fig. 12 Cross-correlation coefficient at various Reynolds number with plasma actuators on: out-of-phase forcing.

To further investigate the effectiveness of the plasma actuators to control the vortex-shedding phase, we also excited the plasma actuators in such a way that the vortex shedding with an arbitrary phase could be obtained. A series of these arbitrary phase shift experiments in the Reynolds number range of 16,700–76,500 demonstrated that the actuators were equally effective in achieving lock-on at any desired phase relationship.

The ability of the plasma actuators to control the vortex-shedding phase depends strongly on the power input besides other factors such as actuator design, flow velocity (Reynolds number), and forcing frequency. Figure 13 shows the effect of input power on the cross-correlation coefficient for a Reynolds number of 41,000 for the configuration-F cylinders. The rms power input to the plasma actuator was calculated using rms of ac voltage and current

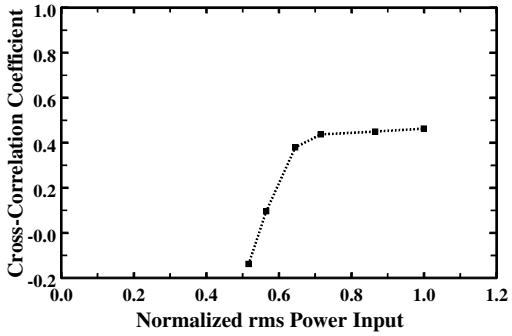

Fig. 13 Effect of power input on correlation coefficient: configuration F, in-phase forcing, $Re_d = 41,000$.

supplied to one pair of electrodes on one side of one cylinder of configuration F. The input power values are normalized with the corresponding level-off (described below) value. Notice that for the lowest power, the cross-correlation coefficient is actually negative and is similar to the unforced case. As the power is increased, the correlation switches to positive and the coefficient's amplitude continues to increase until the coefficient levels off to a plateau at a value of 0.46. This leveling off is probably due to several factors, the first being the limitations in the actuator's design. Because in this configuration, the lower encapsulated electrode is the aluminum cylinder itself, the upper electrode overlaps the lower electrode completely. Asymmetry in the actuator's design is provided only by the fact that its upstream edge is covered by layers of dielectric film; at high enough input power, plasma actually forms under the film and leads to eventual failure of the actuator. Although not as apparent, plasma begins to form in the air at the upstream edge as well, and although not comparable to the downstream jetting caused by the exposed edge of the actuator, it acts as a double dielectric barrier [17] and works against the effectiveness of the downstream edge.

Figure 14 shows the flow visualization of the vortex shedding from the cylinders with configuration E, when the plasma actuators were off, and when they were on. The flow is from left to right and only part of the cylinders, as shown in Fig. 14a, is visible between the shear layers. Figure 14b shows the nominal natural vortex-shedding pattern, the shedding being nominally π out of phase. The flow pattern shows the separated shear layers from each side of the cylinder and the downstream formation of the vortices. Figure 14c shows the images of the flow pattern when the plasma actuators were excited. An important observation is that the flowfield is entirely different from the unexcited case. The separated shear layers are deflected toward the rear stagnation point of the cylinders because of the excitation of the plasma actuators. It appears that the fluid jet, created by the plasma, even penetrated the shear layer on the other side of the cylinder as indicated by the widening of the wake. The phase synchronization of the vortex shedding can be seen by the synchronized jetting at the lower side of each cylinder. The flow visualization on the cylinders with configuration-F plasma actuators is shown in Fig. 15. Figure 15b shows the unexcited vortex shedding again being nominally out of phase. Figure 15c shows the vortex shedding when the plasma actuators were excited. The effect of exciting the plasma actuators can be seen in Fig. 15c where the deflected shear layers have moved closer to the cylinder base.

The mechanism of the interaction between the natural flow on the cylinder and the induced flow of the plasma actuator is still not completely clear, but we believe that the plasma actuator changes the natural shedding to abrupt separation with a jet extending all the way

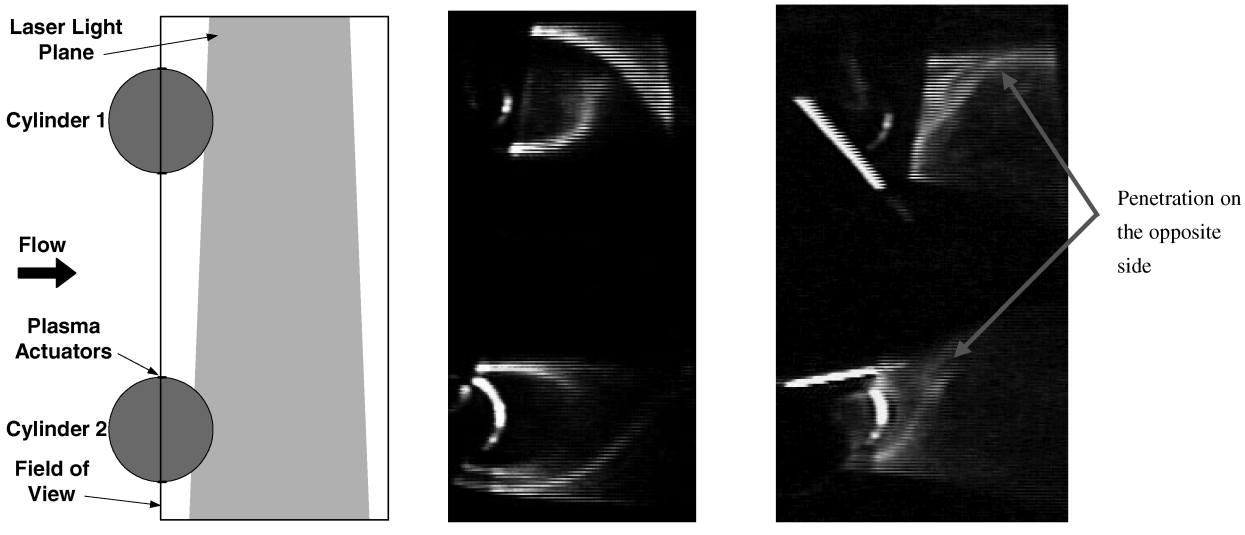

a) Field of view **b) Plasma off** **c) Plasma on**

Fig. 14 Smoke flow visualization at midspan of two side-by-side cylinders: configuration E, $Re = 16,700$, and $P/d = 4$.

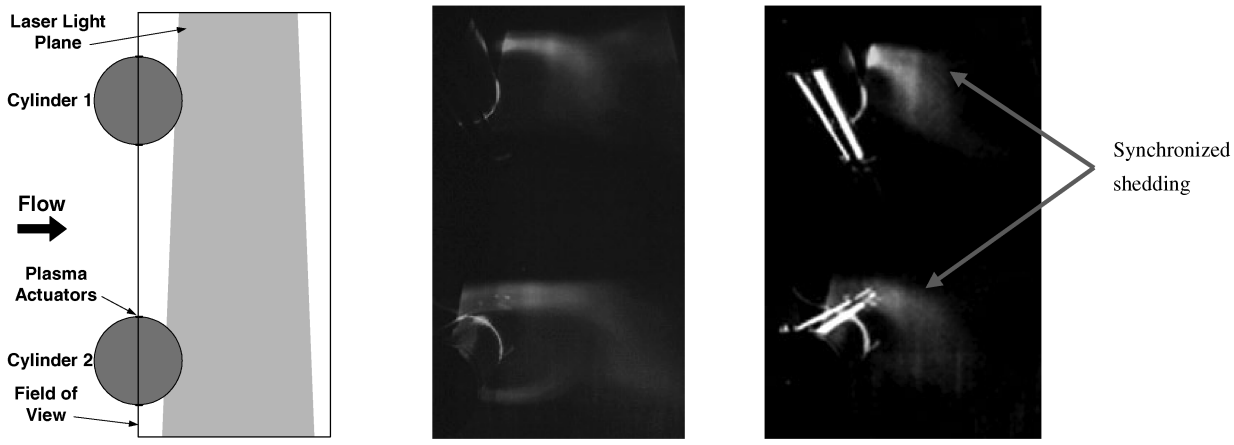

a) Field of view b) Plasma off c) Plasma on

Fig. 15 Smoke flow visualization at midspan of two side-by-side cylinders: configuration F, $Re = 16,700$, and $P/d = 4$.

to the opposite side of the cylinder. This addition of the periodic momentum near the separation point on one side of the cylinder actually forces the shedding of the vortex from the opposite side of the cylinder. Note that in the Reynolds number range of the present tests ($16,700 < Re < 76,500$), the vorticity added to the separated flow causes the vortex from the other side of the cylinder to shed [2,36,37]. Further, the modification of the excited flowfield also depends on the configuration of the plasma actuators as shown by Figs. 14c and 15c, in which excited flowfields are clearly different from each other.

V. Conclusions

Vortex shedding from two side-by-side circular cylinders was phase synchronized in a low-speed flow using plasma actuators up to the target $Re_d = 76,500$. Although the correlation coefficients obtained at $Re_d = 76,500$ were not very high because of the reasons such as the large difference in shedding frequency, the three-dimensional effect, and the formation of plasma at the upstream edge of the exposed electrode, the performance of the actuators to control the vortex shedding in the range $16,700 < Re_d < 76,500$ was good. The ability of the plasma actuators to control the phase of the vortex shedding was also demonstrated by forcing the vortex to shed out of phase and at arbitrary phase. The flow visualization provided the evidence of the synchronization at low Reynolds number.

Acknowledgments

This research effort was jointly sponsored by the U.S. Air Force Research Laboratory/Munitions Directorate, U.S. Air Force Academy, and by the Department of Aerospace and Mechanical Engineering at the University of Notre Dame. The United States government is authorized to reproduce and distribute reprints for governmental purposes not withstanding any copyright notation thereon.

References

[1] Williamson, C. H. K., "Vortex Dynamics in the Cylinder Wake," *Annual Review of Fluid Mechanics*, Vol. 28, No. 1, 1996, pp. 477–539. doi:10.1146/annurev.fl.28.010196.002401

[2] Zdravkovich, M. M., *Flow Around Circular Cylinders, Vol. 1: Fundamentals*, Oxford Science Publications, Oxford, England, U.K., 1997, pp. 3–242.

[3] Giles, E. A., "Low-Dimensional Control of the Circular Cylinder Wake," *Journal of Fluid Mechanics*, Vol. 371, 1998, pp. 157–178. doi:10.1017/S0022112098002122

[4] Sumner, D., Wong, S. S. T., Price, S. J., and Paidoussis, M. P., "Fluid Behaviour of Side-by-Side Circular Cylinders in Steady Cross-Flow," *Journal of Fluids and Structures*, Vol. 13, No. 3, 1999, pp. 309–338. doi:10.1006/jfls.1999.0205

[5] Kim, H. J., and Durbin, P. A., "Investigation of the Flow Between a Pair of Circular Cylinders in the Flopping Regime," *Journal of Fluid Mechanics*, Vol. 196, No. 1, 1988, pp. 431–448. doi:10.1017/S0022112088002769

[6] Fabian, M. K., and Jumper, E. J., "Rearward Forcing of an Unsteady Compressible Cascade," *Journal of Propulsion and Power*, Vol. 15, No. 1, 1999, pp. 23–30. doi:10.2514/2.5413

[7] Fabian, M. K., Falk, E. A., and Jumper, E. J., "Upstream-Propagating Potential Disturbances Interacting with a Compressible Cascade," *Journal of Propulsion and Power*, Vol. 17, No. 2, 2001, pp. 262–269. doi:10.2514/2.5772

[8] Asghar, A., Falk, E. A., Jumper, E. J., Hopper, D. R., and King, P. I., "Unsteady Pressure Response on a Rearward-Forced, Isolated Compressible-Cascade Vane," AIAA Paper 2000-3228, July 2000.

[9] Asghar, A., and Jumper, E. J., "Phase Synchronization of Vortex Shedding from Two Side-by-Side Circular Cylinders Using Plasma Actuators," AIAA Paper 2004-0925, Jan. 2004.

[10] Corke, T. C., and Matlis, E., "Phased Plasma Arrays for Unsteady Flow Control," AIAA Paper 2000-2323, June 2000.

[11] Corke, T. C., Jumper, E. J., Post, M. L., Orlov, D., and McLaughlin, T. E., "Application of Weakly-Ionized Plasmas as Wing Flow-Control Devices," AIAA Paper 2002-0350, Jan. 2002.

[12] Asghar, A., Jumper, E. J., and Corke, T. C., "On the Use of Reynolds Number as the Scaling Parameter for the Performance of Plasma Actuator in a Weakly Compressible Flow," AIAA Paper 2006-0170, Jan. 2006.

[13] Enloe, C. L., McLaughlin, T. E., VanDyken, R. D., Kachner, K. D., Jumper, E. J., and Corke, T. C., "Mechanisms and Responses of a Single Dielectric Barrier Plasma," AIAA Paper 2003-1021, Jan. 2003.

[14] Enloe, C. L., McLaughlin, T. E., VanDyken, R. D., Kachner, K. D., Jumper, E. J., Corke, T. C., Post, M., and Haddad, O., "Mechanisms and Responses of a Single Dielectric Barrier Plasma Actuator: Plasma Morphology," *AIAA Journal*, Vol. 42, No. 3, March 2004, pp. 589–594. doi:10.2514/1.2305

[15] Gibalov, V. I., and Pietsch, G. J., "The Development of Dielectric Barrier Discharges in Gas Gaps and on Surfaces," *Journal of Physics D: Applied Physics*, Vol. 33, No. 20, 2000, pp. 2618–2636. doi:10.1088/0022-3727/33/20/315

[16] Massines, F., Rabehi, A., Decomps, P., Ben Gadri, R., Segur, P., and Mayoux, C., "Experimental and Theoretical Study of a Glow Discharge at Atmospheric Pressure Controlled by Dielectric Barrier," *Journal of Applied Physics*, Vol. 83, No. 6, 1998, pp. 2950–2957. doi:10.1063/1.367051

[17] Finantu-Dinu, E. G., Korzec, D., Teschke, M., and Engemann, J., "Influence of the Electrode Layout on Performance of Insulated Surface Discharge: Electrical Characterization," *Surface and Coatings Technology*, Vols. 174–175, 2003, pp. 524–529. doi:10.1016/S0257-8972(03)00595-4

[18] Enloe, C. L., McLaughlin, T. E., VanDyken, R. D., Kachner, K. D., Jumper, E. J., Corke, T. C., Post, M., and Haddad, O., "Mechanisms and Responses of a Single Dielectric Barrier Plasma Actuator: Geometric Effects," *AIAA Journal*, Vol. 42, No. 3, March 2004, pp. 595–604. doi:10.2514/1.3884.

[19] Wilkinson, S., "Investigation of an Oscillating Surface Plasma for Turbulent Drag Reduction," AIAA Paper 2003-1023, Jan. 2003.

[20] Post, M. L., and Corke, T. C., "Separation Control on High Angle of Attack Airfoil Using Plasma Actuators," AIAA Paper 2003-1024, Jan. 2003.
[21] Huang, J., Corke, T. C., and Thomas, F. O., "Plasma Actuators for Separation Control of Low Pressure Turbine Blades," AIAA Paper 2003-1027, Jan. 2003.
[22] Roth, J. R., and Sherman, D. M., "Boundary Layer Flow Control with a One Atmosphere Uniform Glow Discharge Surface Plasma," AIAA Paper 98-0328, Jan. 1998.
[23] Moreau, E., "Airflow Control by Non-Thermal Plasma Actuators," *Journal of Physics D: Applied Physics*, Vol. 40, No. 3, 2007, pp. 605–636.
doi:10.1088/0022-3727/40/3/S01
[24] Corke, T. C., Post, M. L., and Orlov, D. M., "SDBD Plasma Enhanced Aerodynamics: Concepts, Optimization and Applications," *Progress in Aerospace Sciences*, Vol. 43, Nos. 7–8, Oct.–Nov. 2007, pp. 193–217.
doi:10.1016/j.paerosci.2007.06.001
[25] Pons, J., Moreau, E., and Touchard, G., "Asymmetric Surface Dielectric Barrier Discharge in Air at Atmospheric Pressure: Electrical Properties and Induced Airflow Characteristics," *Journal of Physics D: Applied Physics*, Vol. 38, No. 19, 2005, pp. 3635–3642.
doi:10.1088/0022-3727/38/19/012
[26] Jukes, T. N., Choi, K.-S., Johnson, G. A., and Scott, S. J., "Characterization of Surface Plasma-Induced Wall Flows Through Velocity and Temperature Measurements," *AIAA Journal*, Vol. 44, No. 4, April 2006, pp. 764–771.
doi:10.2514/1.17321
[27] Shyy, W., Jayaraman, B., and Andersson, A., "Modeling of Glow Discharge-Induced Fluid Dynamics," *Journal of Applied Physics*, Vol. 92, No. 11, Dec. 2002, pp. 6434–6443.
doi:10.1063/1.1515103
[28] Orlov, D. M., "Modelling and Simulation of Single Dielectric Barrier Discharge Plasma Actuators," Ph.D. Dissertation, University of Notre Dame, South Bend, IN, 2006.
[29] Font, G. I., "Boundary-Layer Control with Atmospheric Plasma Discharges," *AIAA Journal*, Vol. 44, No. 7, July 2006, pp. 1572–1578.
doi:10.2514/1.18542
[30] Boeuf, J. P., and Pitchford, L. C., "Electrohydrodynamic Force and Aerodynamic Flow Acceleration in Surface Dielectric Barrier Discharge," *Journal of Applied Physics*, Vol. 97, No. 10, 2005, p. 103307.
doi:10.1063/1.1901841
[31] Roy, S., and Gaitonde, D. V., "Force Interaction of High Pressure Glow Discharge with Fluid Flow for Active Separation Control," *Physics of Plasmas*, Vol. 13, No. 2, 2006, p. 023503.
doi:10.1063/1.2168404
[32] Szepessy, S., "On the Control of Circular Cylinder Flow by End Plates," *European Journal of Mechanics, B/Fluids*, Vol. 12, No. 2, 1993, pp. 217–244.
[33] Stansby, P. K., "The Effects of End Plates on the Base Pressure Coefficient of a Circular Cylinder," *Aeronautical Journal*, Vol. 78, 1974, pp. 36–37.
[34] Asghar, A., and Jumper, E. J., "Phase Synchronization of Vortex Shedding from Multiple Cylinders Using Plasma Actuators," AIAA Paper 2003-1028, Jan. 2003.
[35] Asghar, A., "Controlling Shedding from Circular Cylinders Using Plasma Actuators," Ph.D. Dissertation, University of Notre Dame, South Bend, IN, Aug. 2004.
[36] Gerrard, J. H., "The Mechanics of the Formation Region of Vortices Behind Bluff Bodies," *Journal of Fluid Mechanics*, Vol. 25, No. 2, 1966, pp. 401–413.
doi:10.1017/S0022112066001721
[37] Cantwell, B., and Coles, D., "An Experimental Study of Entrainment and Transport in the Turbulent Near Wake of a Circular Cylinder," *Journal of Fluid Mechanics*, Vol. 136, No. 1, 1983, pp. 321–374.
doi:10.1017/S0022112083002189

N. Clemens
Associate Editor